

# Methodology and implementation of bubble-image barometry

Alp Akonur<sup>†‡</sup> and Ajay K Prasad<sup>†</sup>

<sup>†</sup> Department of Mechanical Engineering, University of Delaware, Newark, DE 19716, USA

<sup>‡</sup> Department of Mechanical Engineering, Northwestern University, Evanston, IL 60208, USA

E-mail: prasad@me.udel.edu

Sunrise Setting  
Marked Proof  
MST/106503/PAP  
18727p  
Printed on 22/2/00  
at 12.44

Received 30 July 1999, in final form and accepted for publication 31 January 2000

**Abstract.** The key aspects of a new method, bubble-image barometry (BIB), which can measure both pressure and velocity, are described. BIB extends correlation-based particle-image velocimetry techniques to provide simultaneous pressure and velocity measurements over a global domain. The particles used in BIB (gas bubbles) serve two purposes: (i) they are small enough to track the flow and serve as tracers for the velocity field; and (ii) they behave as local pressure sensors by changing their size in response to the instantaneous pressure field. The present work explores the theoretical and practical issues involved in BIB by first introducing the relation between the bubble-image size and its spatial correlation function. Next, computer-generated bubble images are used to investigate the feasibility of the technique. Finally, a pressure-chamber experiment, wherein microscopic air bubbles are generated and used as tracer particles to measure pressure, is presented. Results obtained from the experiment show that BIB is a viable technique for a certain range of bubble sizes.

**Keywords:** bubbles, whole-field pressure measurement, whole-field velocity measurement, simultaneous velocity and pressure measurement, particle-image velocimetry, bubble-image barometry, pressure measurement, flow measurement

## 1. Introduction

In recent years, reliable velocity measurements in turbulent flow fields have been made using particle-image velocimetry (PIV) [1] and digital particle-image velocimetry (DPIV) [2]. Similarly, instantaneous temperature measurements have been made on global domains using thermochromic liquid crystals [3].

Although techniques such as use of pressure-sensitive paints provide global pressure data on solid surfaces, there is no method for measuring whole-field pressures *within* a flow field. Current methods require the use of pressure transducers which do not give reliable information because their size is often comparable to the size of the small scales of motion. Furthermore, such measurements are at best pointwise and intrusive. Kim [4] attributes our lack of understanding of pressure fluctuations in turbulent flows to the unavailability of a pressure-measurement technique comparable to modern techniques for measuring turbulent-velocity fluctuations. The ability to obtain pressure simultaneously with velocity is critical to the closure problem of turbulence modelling which persists because there is still no way to globally measure the pressure–strain correlation; the pressure–strain correlation involves both velocity and pressure fluctuations.

The idea of using bubbles for non-intrusive pressure measurements is not new. For example, specially tailored air bubbles were utilized as static pressure sensors by Ooi

and Acosta [5]. The authors described the conditions under which air bubbles of a certain size accurately reflect the local static pressures. Later, another detailed investigation of the response of microscopic bubbles to sudden changes in ambient pressure was performed by Ran and Katz [6]. Their investigation included the effects of various gases such as air, hydrogen, helium and carbon dioxide. As a result of their experiments, the authors were able to show that the microscopic bubbles, varying in size from 90 to 400  $\mu\text{m}$  in diameter, respond ‘instantaneously’ to sudden changes at a rate of 20 kPa  $\text{ms}^{-1}$ . Later, air bubbles were used further in other applications such as the measurement of pressure fluctuations and their effect on inception of cavitation within water jets [7] and measurement of drag and lift forces on microscopic bubbles entrained by a vortex [8]. In these investigations, the holography technique was used. The bubble-size measurements were made on the reconstructed images by magnifying them optically by a factor of about 500 and then measuring the bubble sizes manually one by one on a monitor.

In the present work, we describe the bubble-size determination and corresponding pressure measurement of a new technique, bubble-image barometry (BIB). BIB differs from previous techniques in two significant ways: (i) the bubble diameter, and therefore pressure, is obtained in an automated manner together with the velocity without the need for man-

ual measurement; and (ii) pressures and velocities can be obtained simultaneously so that it will be possible, for the first time, to overlay instantaneous pressure and velocity fields.

It is important to note that our goal in this paper is to demonstrate that pressure measurements can be obtained as a by-product of the PIV process. Many studies have already proved that PIV can provide accurate velocity information over global domains. Hence, we measure only pressure and show that BIB extends PIV by providing simultaneous pressure information with little additional computation. The ultimate goal of performing simultaneous pressure and velocity measurements is an on-going effort and will be reported at a later date.

## 2. Particle-size determination

The heart of the BIB technique resides in the spatial-correlation process which provides not only the displacement of bubbles (PIV) but also an estimate of the bubble diameter. The spatial correlation of the PIV interrogation spot yields the displacement vector corresponding to the average displacement of all particles contained in this spot. Similarly, if bubbles are used as tracer particles, the pressure obtained after interrogation will represent the average pressure of all the bubbles contained in the same interrogation spot.

BIB exploits the direct relation between the size of the particle image and the size of the self-correlation peak (figure 1). Let the image intensity function over an interrogation spot be represented by  $I(x)$  where  $x$  defines a two-dimensional space. The auto-correlation function  $R(s)$  of  $I(x)$  is given by

$$R(s) = \int_{spot} I(x)I(x+s) dx \quad (1)$$

where  $s$  is the two-dimensional shift of the intensity function. It is possible to evaluate equation (1) by taking the Fourier transform of the image data using the convolution theorem

$$R(s) = F^{-1}\{[F[I(x)]]^2\} \quad (2)$$

where  $F$  is the two-dimensional Fourier transform.

To illustrate the relation between the size of a single particle image and the size of its correlation function, consider a Gaussian particle image whose intensity function takes the form

$$I(x) = \frac{1}{\sigma(2\pi)^{1/2}} \exp\left(\frac{-x^2}{2\sigma^2}\right). \quad (3)$$

The diameter of the particle scales with the standard deviation of the Gaussian distribution  $\sigma$  (typically  $4\sigma$  is used to represent the effective particle diameter).

When  $R(s)$  is calculated via equation (2) analytically, one obtains

$$\sigma_{sc} = \sqrt{2}\sigma \quad (4)$$

where  $\sigma_{sc}$  is the standard deviation of the self-correlation peak. Equation (4) proves the existence of the direct relation between the radius of the particle image and the radius of the self-correlation peak. Similarly, if one computes the spatial correlation of a collection of particle images within a

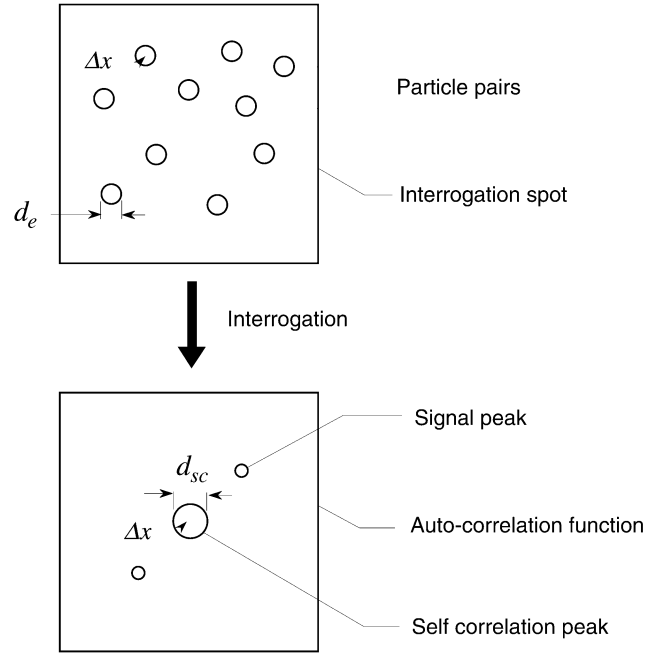


**Figure 1.** The relation between the sizes of the bubbles and the self-correlation peak.

single interrogation spot, it can be proved that the diameter of the self-correlation peak is directly related to the *average* diameter of all the contributing particle images.

It is important to note that the recorded particle-image size may be modified by diffraction effects. The true size of the bubble  $d_p$  maps onto the effective image diameter  $d_e$  on the recording medium according to [9]

$$d_e = (M^2 d_p^2 + d_s^2)^{1/2}. \quad (5)$$

Here,  $M$  is the magnification and  $d_s$ , the diffraction-limited spot size [1], is given by

$$d_s = 2.44(1 + M)f\lambda. \quad (6)$$

For  $\lambda = 532$  nm (the wavelength of a frequency-doubled Nd:Yag laser), with  $f$  number of recording optics  $f/8$  and  $M = 1.0$ , we obtain  $d_s = 20.7$   $\mu\text{m}$ . It can be inferred that diffraction theory should certainly be taken into account when  $Md_p$  is comparable to  $d_s$ . However, if  $Md_p \gg d_s$ , then equation (5) reduces to

$$d_e = Md_p. \quad (7)$$

The intensity function,  $I(x)$ , strongly depends upon (i) the size of the particle, (ii) the illumination of the flow field and (iii) recording parameters (the  $f$  number, magnification, type of recording medium and/or dark-room chemistry). These effects limit the particle-size range in which measurements can be performed. In order to explore the particle-size range for which deformations of bubbles could reliably be measured, a test with computer-generated particles plotted on paper was performed. The computer program PGPLOT provided a means of varying the parameters of concern, namely the size and the number density of the particles. The size of the particles ranged from 100 to 500  $\mu\text{m}$ . The number density of particles in

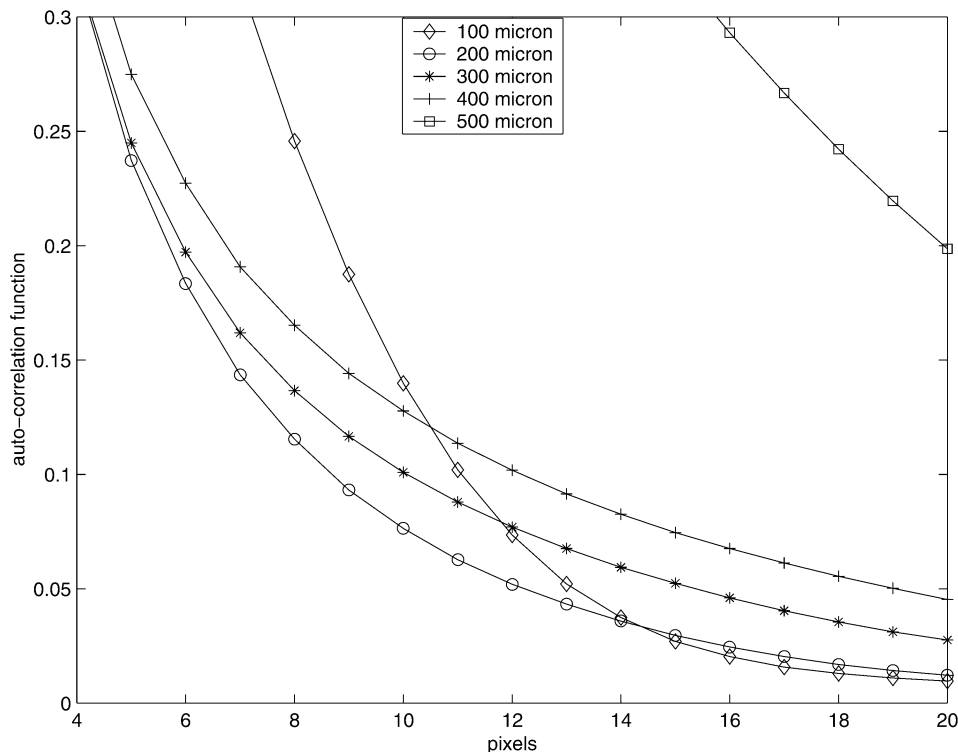


**Figure 2.** A close-up view of the self-correlation curves obtained from computer-generated particles.

a picture varied from 2 to 5 particles  $\text{mm}^2$  according to their size. The plots obtained from the computer program were photographed by a Nikon F3 camera on TMAX 100 black and white film at  $M = 0.48$  and  $f/8$ . The 35 mm film was digitized at a resolution of  $106 \text{ pixels mm}^{-1}$ . The auto-correlation was calculated with an interrogation spot size of 128 pixels by 128 pixels. The self-correlation peak provided the bubble size as described previously. This procedure was repeated for differently sized particles. Figure 2 shows the self-correlation functions. It is seen that, for particle diameters between 200 and 400  $\mu\text{m}$ , the curves behave smoothly in proportion to the particle sizes. However, for the ones outside this range (100 and 500  $\mu\text{m}$ ) this is not true. The range within which the curves exhibit the desired behaviour is limited by two parameters: (i) the interrogation spot size and (ii) the resolution of the image (pixel size). The interrogation-spot size constitutes the upper bound. If the particle diameter is comparable to the interrogation-spot size, the probability that the particle is truncated by the edges of the interrogation spot is large. In such a case, the particle diameter cannot be determined correctly. On the other hand, the smallest particle diameter that can be measured is limited by the resolution provided by the scanner, which in our case was  $106 \text{ pixels mm}^{-1}$ . As a result, only the particle diameters within these limits can reliably be measured. It must be noted that these limits are specific to the hardware used in the current work.

### 3. Bubble generation

BIB requires that the flow be supplied with a sufficient concentration of bubbles of very uniform size. This requirement should be satisfied in order to obtain reliable

pressure measurements by comparing the bubble diameter at later times with the initial bubble diameter (during generation) at a known pressure. Among many bubble-generation techniques, the one proposed by Oguz and Prosperetti [10], by use of a needle, was found to be suitable for the purposes of this experiment. According to their model, two parameters influence the observed bubble diameter at the time of detachment of a bubble from the end of the needle: (i) the critical air flow rate through the needle ( $Q_{cr}$ ) and (ii) the equilibrium bubble radius ( $R_F$ ).  $R_F$  is determined by the balance between buoyancy forces and surface tension forces during detachment:

$$R_F = \left( \frac{3\gamma a}{2\rho_l g} \right)^{1/3} \quad (8)$$

where  $\gamma$  is the surface tension,  $a$  is the inner radius of the needle,  $\rho_l$  is the density and  $g$  is the acceleration due to gravity. The model suggests that, if the air flow through the needle is below a limiting value,  $Q_{cr}$ ,

$$Q_{cr} = \pi \left( \frac{16}{3g^2} \right)^{1/6} \left( \frac{\gamma a}{\rho_l} \right)^{5/6} \quad (9)$$

then all the bubbles generated will detach from the needle with the same equilibrium size, given by equation (8). However, if the air-flow rate is larger than the critical value, the volume of the bubbles will be proportional to  $Q^{5/6}$ .

The bubble-generating system consisted of a glass capillary tube and the air-supply line. It was arranged such that the bubbles were generated in a quiescent medium. The bubble generator was placed in a tube long and large enough to make sure that the bubbles generated were not affected by the walls of the tube and the fluid flow in the box where the bubbles were allowed to accumulate.

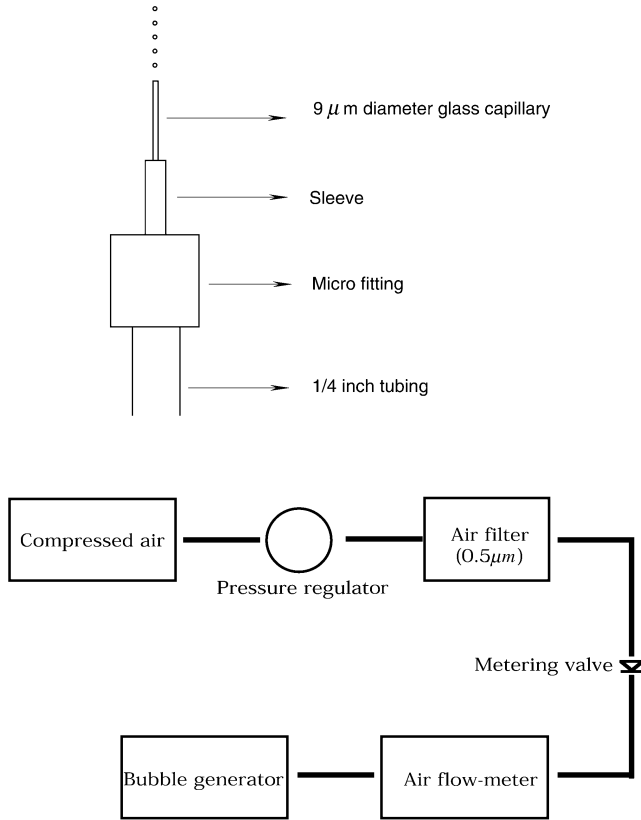


**Figure 3.** The bubble-generator-circuit assembly, showing the capillary device (top) and the air-supply circuit (bottom).

The capillary was a flexible fused silica tube of  $9 \mu\text{m}$  inner diameter and  $150 \mu\text{m}$  outer diameter. It was held in a sleeve by a finger-tight fitting arrangement which was itself connected to the main air line by a column coupler and 0.25 in PFA tubing. This arrangement was especially successful at preventing leakage. The above assembly was incorporated into a circuit as shown in figure 3. The circuit consisted of a pressure regulator, a  $0.5 \mu\text{m}$ -pore-size air filter, a metering valve and a flow meter capable of measuring small air-flow rates. Figure 4 is a photograph of the bubble generator in operation and demonstrates the uniformity obtained with the system. It was observed that the technique was highly reproducible at producing bubbles of the same size as long as the same air-flow rate was supplied through the same needle. In figure 4,  $Q_{cr} = 0.75 \text{ cm}^3 \text{ min}^{-1}$ ,  $R_F = 283 \mu\text{m}$  and the surrounding fluid was mineral oil with  $\gamma = 28.9 \times 10^{-3} \text{ N m}^{-1}$ ,  $\mu = 0.074 \text{ Pa s}$  and  $\rho = 875 \text{ kg m}^{-3}$ .

One possible difficulty with using bubbles as pressure sensors arises due to diffusion of dissolved gas from the liquid into the bubble, or from the bubble into the liquid. However, it had previously been reported that even a thin layer of oil around an air bubble greatly alters the mass transfer of air into or out of the bubble [11]. Noting that mineral oil was used as the medium in which bubbles were generated, it is reasonable to expect a negligible amount of mass transfer due to the concentration of dissolved air in oil. Then, for an isothermal process, the initial bubble diameter can be related to the one at a later time via

$$R^3 + \frac{2\gamma}{P_\infty} R^2 - \frac{P_{g0}}{P_\infty} R_0^3 = 0 \quad (10)$$



**Figure 4.** The bubble generator in operation.

where

$$R_0 = R_F$$

$$P_{g0} = P_{\infty 0} + 2\gamma/R_0. \quad (11)$$

In equation (10),  $P_\infty$  and  $R$  represent the local pressure and corresponding bubble radius, while  $P_{\infty 0}$  and  $R_0$  represent the pressure and bubble radius during bubble generation. Knowing  $R$ ,  $R_0$  and  $P_{\infty 0}$ , one can thus determine the local pressure,  $P_\infty$ .

#### 4. Experimental details

The experimental set-up consisted of a rectangular chamber made of Plexiglas with three glass windows as shown in figure 5. Air bubbles were generated inside the bottom extension tube. After the bubbles had been generated at an initial pressure (and diameter), their diameter was altered by varying the pressure in the box. The photographs of bubbles were recorded and the auto-correlation functions were computed. The superposed pressure inside the chamber was known independently; this provided a good check on the pressure measurement based on bubble diameter.

The base of the box was a 19 mm-thick square plate with 12.7 cm sides and 25.4 cm height. The glass windows were of sizes 2.54 cm by 10.2 cm on the side walls and 7.6 cm by 7.6 cm on the front. The side windows allowed the light to pass through the box and illuminate the fluid. The front window was used for recording images. O rings were used to seal the windows and the top of the box, which was removable. The seal allowed the box to be pressurized and evacuated. The top of the box had ports for the vacuum pump and for the main compressed-air line. The range of possible pressures was from 0.33 to 1.68 bar (absolute). The

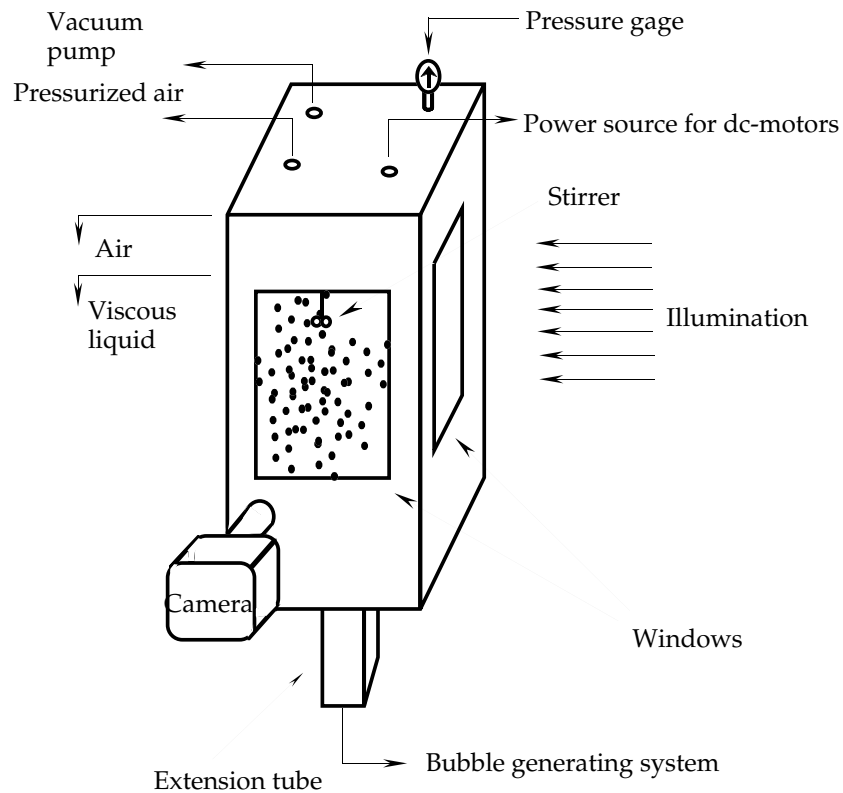


**Figure 5.** The experimental set-up.

compressed-air line was split into two by a T junction; one line went to the bubble generator and the other went to one of the ports to pressurize the box. The bubble generator was attached to the bottom of the box so that the bubbles formed a vertical line from the tip of the capillary to the surface of the oil.

Because the maximum pressure that could be safely attained in our chamber was around 1.8 bar (absolute), large pressure ratios could be obtained only by generating bubbles at an initial pressure below 1 bar (absolute). Thus, the initial pressure was 0.33 bar in all cases. Noting that all the pressures given are absolute, the pressure ratio  $P_2/P_1$  ranged between 1 and 5.1. After the box had been evacuated down to 0.33 bar, the air flow was supplied to the capillary at a flow rate which yielded bubbles  $850 \mu\text{m}$  in diameter at a rate of  $4\text{--}5 \text{ bubbles s}^{-1}$ . The terminal rise velocity of the bubbles was about  $2.1 \text{ mm s}^{-1}$ . The requirement for bubble-size uniformity was adequately satisfied via equation (9). The pressure, which had initially been 0.33 bar, was increased in steps and, with each increment of pressure, new pictures were taken by a Nikon F3 camera on TMAX 100 black and white film at  $f/8$ . The magnification was 0.5, so that the bubbles on the image plane were obtained with a maximum diameter of  $425 \mu\text{m}$ . In this manner, the bubble-size range matched that in section 2. The 35 mm negatives were developed and scanned at a resolution of  $106 \text{ pixels mm}^{-1}$ . The digitized portion of the negative contained the vertical line of closely spaced bubbles. Bubble images captured at three different pressures can be seen in figure 6. The width of the digitized strip was equal to 128 pixels, which was also the horizontal dimension of the interrogation spot. Each interrogation spot contained two bubble images on average. Fresh bubbles

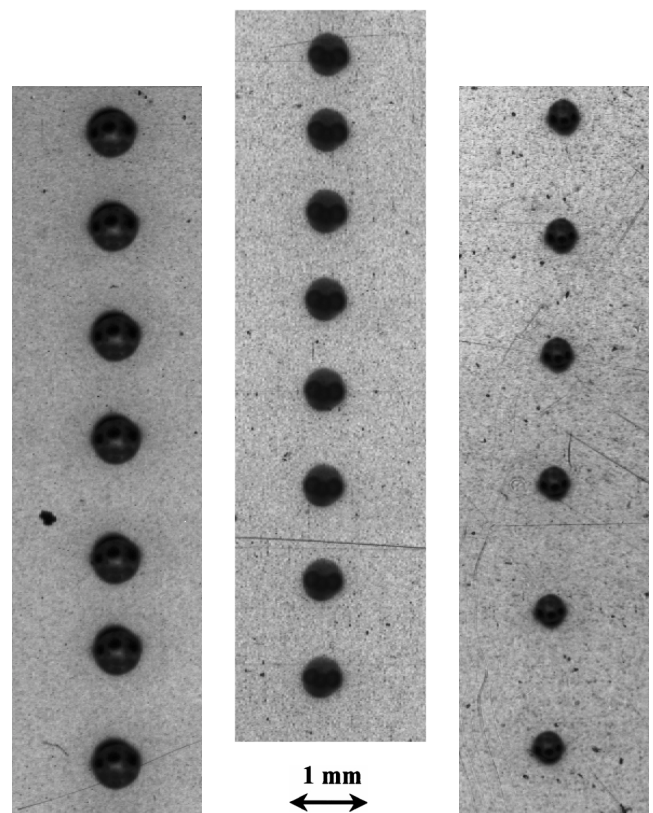


**Figure 6.** Sample images of bubbles under pressure: 0.33 bar (left-hand side), 1.00 bar (centre) and 1.34 bar (right-hand side).

were generated at an initial pressure of 0.33 bar for each new measurement at an increased final pressure. 36 observations were used to obtain each data point.

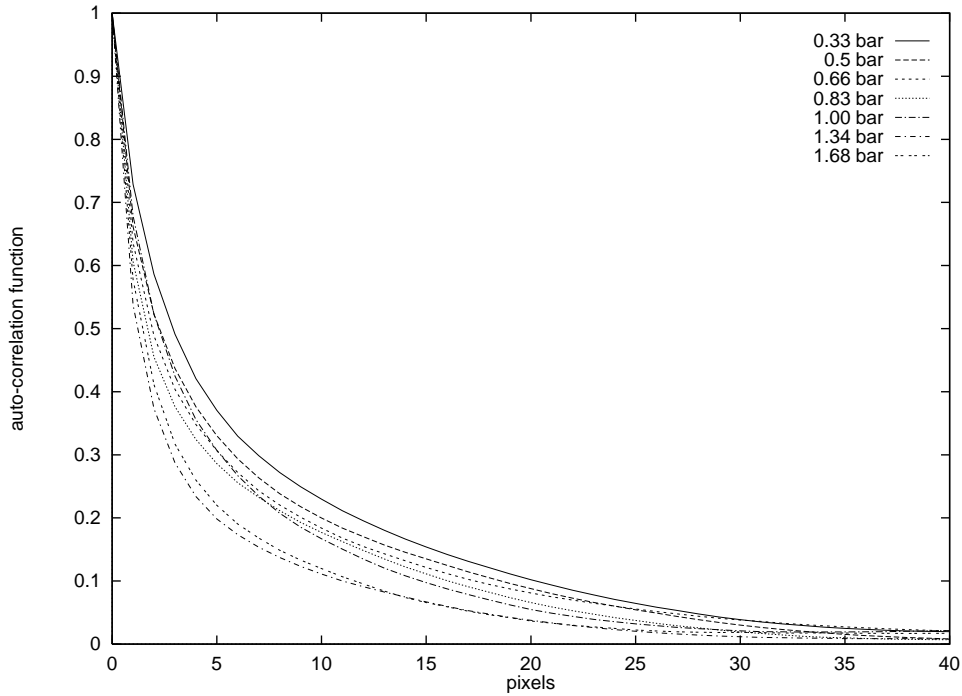


Figure 7. Self-correlation curves obtained at various pressures.

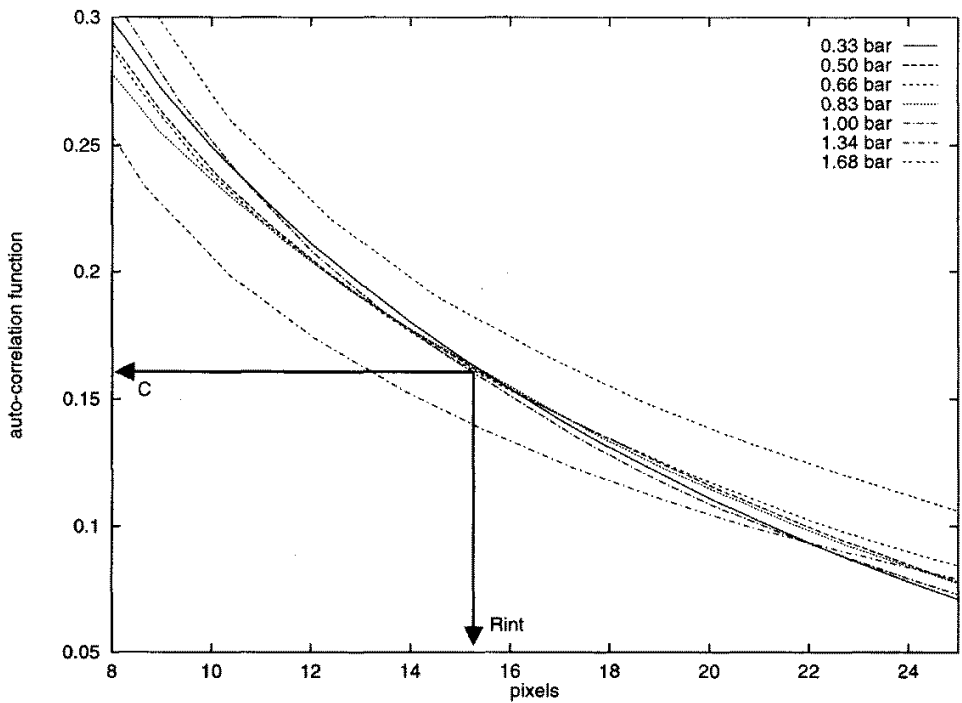


Figure 8. A close-up of the region of intersection of normalized self-correlation curves.

### 5. Results

Given the bubble images recorded at various predetermined chamber pressures, the bubble sizes were obtained in two ways: (i) using the auto-correlation function as described earlier and (ii) by manually measuring the bubble-image diameter under a microscope.

Correlation curves for each bubble size were plotted on the same graph by first normalizing the  $x$ -axis for each curve with the corresponding bubble size (which is in this case known *a priori*). In the ideal case, all curves would collapse

exactly onto one another. However, such a collapse was not possible owing to the nature of our experiment. For our purpose, it is sufficient if the curves display a point or a small region at which the curves intersect or overlap. Let us denote the normalized radial location of this point or region as  $R_{int}$  and the corresponding correlation value as  $c$ . Of course, it is possible to rescale the  $x$ -axis such that  $R_{int}$  directly corresponds to the reference bubble radius in the physical domain (fluid). Then, for any bubble of unknown radius, it is possible to plot its non-normalized correlation function on

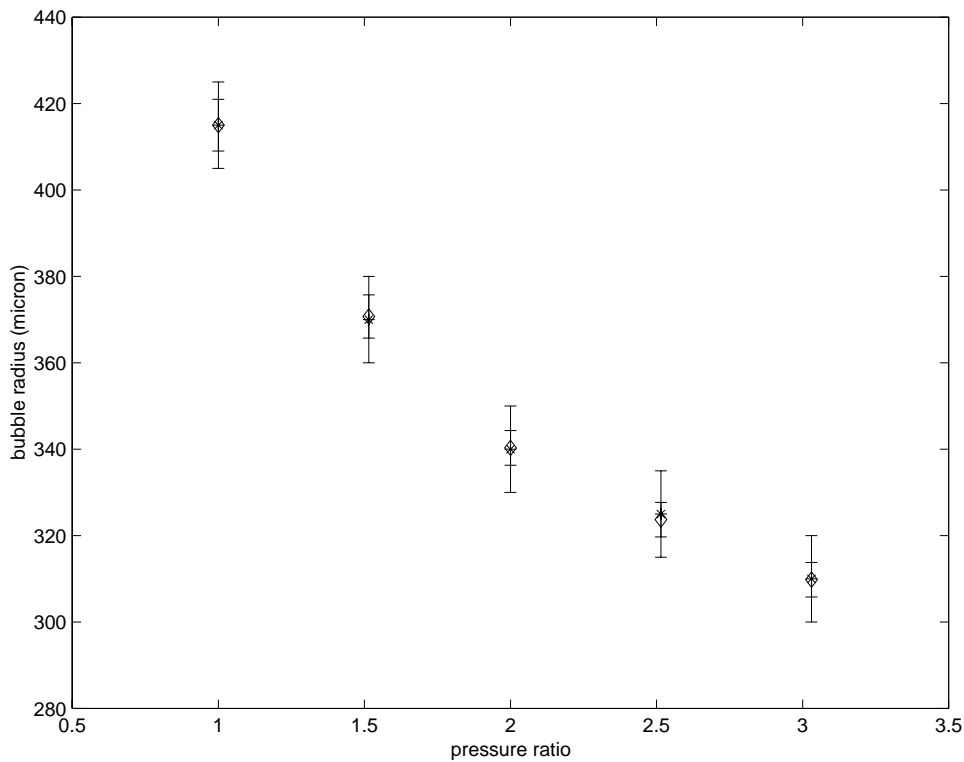


**Figure 9.** A comparison of bubble sizes obtained by using BIB ( $\diamond$ ) and the manual method (\*).

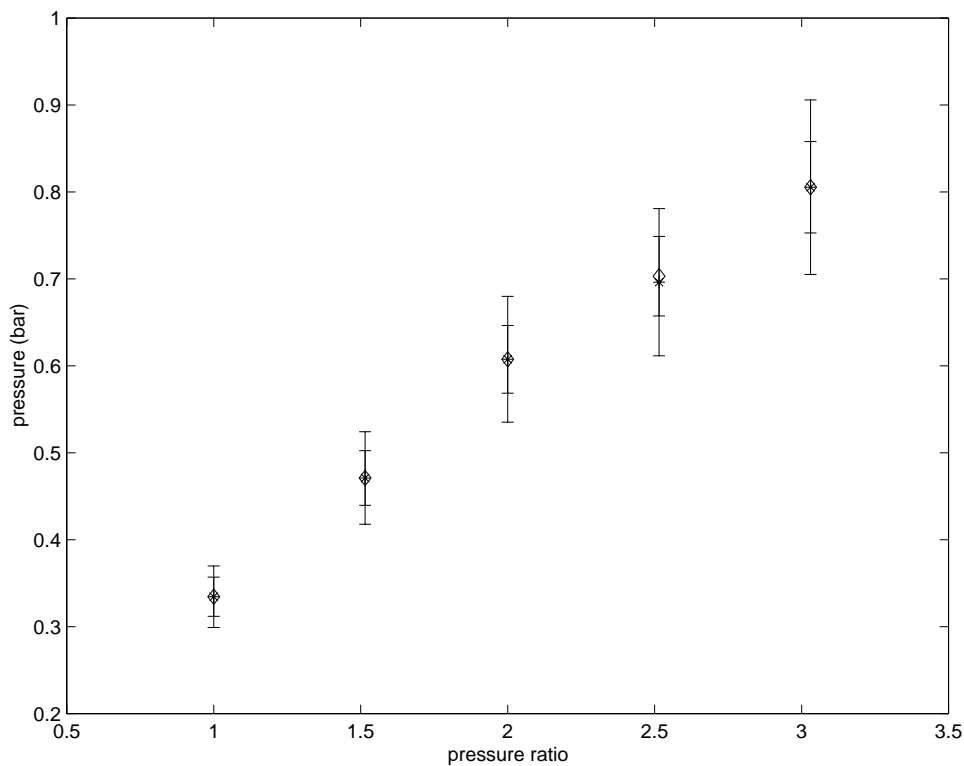


**Figure 10.** A comparison of pressures obtained by using BIB ( $\diamond$ ) and the manual method (\*).

the same plot and read off the radial location corresponding to a correlation value of  $c$ . This value is the desired bubble radius.

Figure 7 shows the radius of the self-correlation peak changing in proportion to the radius of the bubbles. Figure 8 shows the same results after the correlation curves had been normalized. The values of  $c$  and  $R_{int}$  were 0.165 and

15 pixels respectively. As long as the experimental conditions remain identical, the same value of  $c$  can be used to obtain bubble diameters from normalized auto-correlation curves. Figure 8 reveals that, for pressure ratios 4.1 (1.34 bar) and 5.1 (1.68 bar), the curves did not fall within the region of intersection. Therefore, the values obtained from them will not give reliable results for bubble diameter and pressure.

This implies that BIB measurements were accurate for changes in bubble diameter within 30% of the initial bubble diameter for the chosen conditions of this experiment.

The bubble diameter and pressure were calculated for pressure ratios from 1 to 3.0. The bubble diameters obtained from the auto-correlation peaks were used in equation (10) to calculate the corresponding pressures. The bubble radius and the chamber pressure at the time the bubbles were generated were taken as the initial conditions. The results are plotted in figures 9 and 10.

It can be seen that the bubble radius and pressure values obtained from BIB agree very well with the values obtained from manual measurements performed under the microscope. Such good agreement is the result of locating the calibration point ( $c$ ) precisely and thus avoiding relative variation between the auto-correlation curves. The accuracy of  $c$  depends on the smallness of the region of intersection. In addition, the uncertainty in pressure measurements increases for higher pressure ratios, indicating that it is necessary to perform very accurate bubble-diameter measurements in order to obtain reliable pressure measurements.

## 6. Summary

The theoretical and experimental feasibility of performing instantaneous, global pressure measurements was investigated. This new technique, named bubble-image barometry (BIB), extends standard PIV by using small gas bubbles as tracer particles to serve two purposes. First, bubble displacement provides the local fluid velocity by standard PIV methods. Second, the average diameter of all bubbles contained within an interrogation spot provides the local pressure. Analytical considerations reveal that information about the bubble diameter is preserved while calculating the spatial auto-correlation function. Consequently, it is possible to obtain the average diameter of small groups of bubbles together with their average displacement without additional computation.

Experiments were conducted using computer-generated images to test the validity of the theory and explore a suitable range of particle diameters over which BIB would succeed for the given experimental hardware. Finally, pressure-chamber experiments using air bubbles as tracer particles proved that, for a certain range of bubble diameter, it is possible to measure pressure reasonably accurately as a by-product of PIV.

Although BIB provides a new way of performing simultaneous pressure and velocity measurements, improvements on three fronts will ensure its applicability to a wide variety of challenging problems.

- (i) Bubble generation. Accurate velocity measurement requires the use of small tracer particles (bubbles in the case of BIB). However, generation of small and uniformly sized bubbles in large amounts poses practical difficulties. With the bubble-generation methods currently available, only one of these two conditions can be successfully satisfied.
- (ii) Determination of the bubble diameter. From figures 9 and 10, it is observed that the error in the pressure measurement is approximately three times larger than the error in the bubble-diameter measurement owing

to the fact that  $p \sim D^{-3}$ , where  $D$  is the bubble diameter. Therefore, accurate determination of the bubble diameter is extremely important for successful BIB measurements.

- (iii) Mass-transfer effects. First, the present experiments were performed in pure mineral oil. Second, the pressure changes in the chamber did not result in oscillations. These two considerations ensured that mass transfer into and out of the bubble during the experiments was minimal. However, for common liquids such as water, this might not always hold true. Equation (11) would then have to be modified to include such effects.

Advances in technology will undoubtedly allow us to overcome these limitations. For example, micro-electro-mechanical systems (MEMS) devices may provide a way to rapidly generate large quantities of extremely uniform bubbles. Similarly, holographic techniques (HPIV) will allow determination of the bubble diameter with greater accuracy and perhaps also extend the range of measurement. The continual improvement in performance and cost-effectiveness of imaging hardware will also allow greater automation and make implementation of BIB easier.

## Acknowledgment

We wish to thank the University of Delaware, Department of Mechanical Engineering, for supporting this project by providing a graduate assistantship.

## References

- [1] Adrian R J 1993 Particle-imaging techniques for experimental fluid mechanics *Ann. Rev. Fluid Mech.* **23** 261–304
- [2] Willert C E and Gharib M 1991 Digital particle image velocimetry *Exp. Fluids* **10** 181–93
- [3] Dabiri D and Gharib M 1991 Digital particle image thermometry: the method and implementation *Exp. Fluids* **11** 77–86
- [4] Kim J 1989 On the structure of pressure fluctuations in simulated turbulent channel flow *J. Fluid Mech.* **205** 421–51
- [5] Ooi K K and Acosta A J 1984 The utilization of specially tailored air bubbles as static pressure sensors in a jet *J. Fluids Engng* **106** 459–65
- [6] Ran B and Katz J 1991 The response of microscopic bubbles to sudden changes in the ambient pressure *J. Fluid Mech.* **224** 91–145
- [7] Ran B and Katz J 1994 Pressure fluctuations and their effect on cavitation inception within water jets *J. Fluid Mech.* **262** 223–63
- [8] Sridhar G and Katz J 1995 Drag and lift forces on microscopic bubbles entrained by a vortex *Phys. Fluids* **7** 389–99
- [9] Adrian R J and Yao C 1985 Pulsed laser technique application to liquid and gaseous flows and the scattering power of seed materials *Appl. Opt.* **24** 44–52
- [10] Dynamics of bubble growth and detachment from a needle *J. Fluid Mech.* **257** 111–45
- [11] Gowing S 1987 Dissolving of bubble in a liquid. Report to David W Taylor, Naval Ship Research and Development Center